CHEMISTRY
A EUROPEAN JOURNAL

DOI: 10.1002/chem.200801654

Distinct Hydroxy-Radical-Induced Damage of 3′-Uridine Monophosphate in RNA: A Theoretical Study

Ru bo Zhang[a, b] and Leif A. Eriksson*[b]

Abstract: RNA strand scission and base release in 3′-uridine monophosphate (UMP), induced by OH radical addition to uracil, is studied at the DFT B3LYP/6-31+G(d,p) level in the gas phase and in solution. In particular, the mechanism of hydrogen-atom transfer subsequent to radical formation, from C2′ on the sugar to the C6 site on the base, is explored. The barriers of (C2′-)H2′$_a$ abstraction by the C6 radical site range from 11.2 to 20.0 kcal mol^{-1} in the gas phase and 14.1 to 21.0 kcal mol^{-1} in aqueous solution, indicating that the local surrounding governs the hydrogen-abstraction reaction in a stereoselective way. The calculated N1−C1′ (N1–glycosidic bond) and β-phosphate bond strengths show that homolytic and heterolytic bond-breaking processes are largely favored in each case, respectively. The barrier for β-phosphate bond rupture is approximately 3.2–4.0 kcal mol^{-1} and is preferred by 8–12 kcal mol^{-1} over N1–glycosidic bond cleavage in both the gas phase and solution. The β-phosphate bond-rupture reactions are exothermal in the gas phase and solution, whereas N1−C1′ bond-rupture reactions require both solvation and thermal corrections at 298 K to be energetically favored. The presence of the ribose 2′-OH group and its formation of low-barrier hydrogen bonds with oxygen atoms of the 3′-phosphate linkage are highly important for hydrogen transfer and the subsequent bond-breakage reactions.

Keywords: density functional calculations · nucleic acids · radicals · RNA · solvent effects

Introduction

Radical attack is one of the main reasons behind nucleic acid damage.[1] Electron paramagnetic resonance (EPR) spectroscopy experiments in conjunction with spin-trapping carried out in aqueous solution have shown that ·H, ·OH, and alkoxy radicals can add to the C5=C6 double bond of the pyrimidine bases. The ·OH radical adducts of the pyrimidines at either C5 or C6 have both oxidizing and reducing capabilities.[2] Furthermore, a competing set of reactions is posed by hydrogen-atom abstraction by the ·OH radical from the sugar moiety in nucleosides, nucleotides, and nucleic acids (NAs).[3–5] These depend on the C−H bond strength and lead to alteration of the sugar moiety and subsequent rearrangements that in turn have been suggested to generate base release or strand break.[6]

It is generally accepted that nucleobase–radical adducts contribute to strand break.[7–9] The exact mechanism is, however, uncertain to date. EPR results have indicated this to be a slow process,[10] with the rate-limiting step suggested to involve intra- or intermolecular hydrogen-atom abstraction from a sugar moiety (paths A and C in Scheme 1).[11] This process has also been suggested to proceed by way of initial protonation of the radical adduct, followed by dehydration to form a radical cation, intramolecular H transfer, and strand scission (path B of Scheme 1).[12] The mechanism involving intranucleotide hydrogen-atom abstraction, as well as the protonation/dehydration pathway, have been proposed to be less important in the biopolymer, owing to the stability of the nucleobase–radical adduct.[13] It is evident that the above processes are often quenched in the presence of molecular oxygen, although they have been reported to occur in hypoxic cells.[7]

Experimental and theoretical results have shown that rupture of the N1–glycosidic bond can be caused by a cationic C6 lesion that arises as a result of one-electron removal from the 5,6-dihydro-6-thymyl radical,[14] whereas the capture of an excess electron by the cytosine N3−H atom radi-

[a] Dr. R. b. Zhang
The Institute for Chemical Physics and School of Science
Beijing Institute of Technology, Beijing 100081 (China)

[b] Dr. R. b. Zhang, Prof. L. A. Eriksson
Örebro Life Science Center, School of Science and Technology
Örebro University, 701 82 Örebro (Sweden)
E-mail: leif.eriksson@oru.se

Supporting information for this article is available on the WWW under http://dx.doi.org/10.1002/chem.200801654.

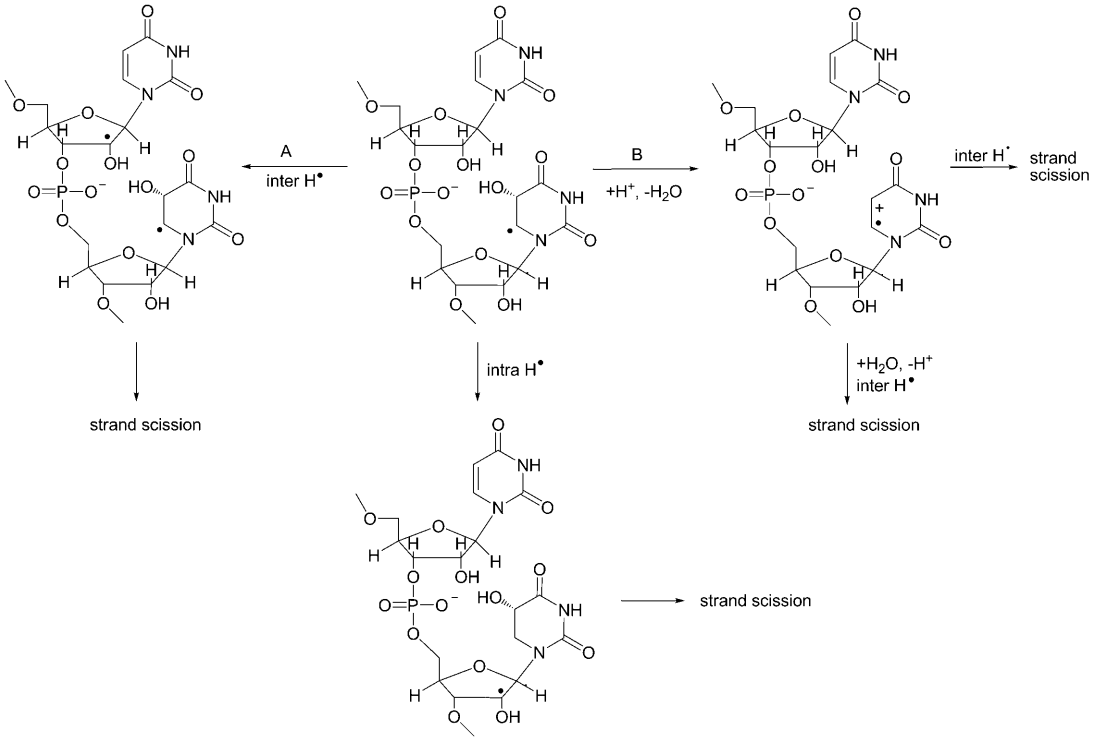

Scheme 1. Strand break illustrated through a rate-limiting step that may involve intra- or intermolecular hydrogen-atom abstraction from a sugar moiety through two varied pathways (path A or B).

cal adduct leads to the automatic rupture of the β-phosphate bond.[15] Our previous calculations[16,17] have shown that the barriers of hydrogen transfer from C2′ on the sugar moiety to C6 on the radical-modified thymine base range from 21 to 24 kcal mol^{-1}. Subsequent ruptures of N1–glycosidic and β-phosphate bonds are not formed directly through hydroxy or hydrogen addition to the C5=C6 bond owing to the high stability of the free-radical complexes. The bond ruptures can, however, occur in the electron adducts, in which case the β-phosphate bond is more facile to be broken than the N1–glycosidic bond. The bond ruptures resulting from interaction of low-energy electrons with DNA have also been observed by other authors.[18–22] The data indicate that injection of negative charge is sufficient to cause DNA strand break. The hydroxy group covalently bound to C2′ of ribose is the main characteristic of ribonucleotides/RNA that is different from deoxyribonucleotides/DNA. This group plays a significant role in some certain reactions, such as RNA catalysis.[23] The work reported herein primarily refers to 3′-uridine monophosphate (3′-UMP; Scheme 2), which can be expected to display similar structures and properties to 3′-dTMP (dTMP = thymidine monophosphate) and is employed herein to model the 5′ terminal of the RNA strand. Given the complex and asymmetric local environment, both back and front attack at the C5 site of the base by ·OH radicals are considered. In particular, the process of carbon-centered H-atom transfer from C2′ on the ribose moiety to C6 on the radical-modified uracil base, and the subsequent strand breakage reactions are explored in detail. The bond dissociation energies (BDEs) and activation barriers of the β-phosphate and N1−C1′ (N1–glycosidic) bonds are calculated to investigate possible cleavage modes

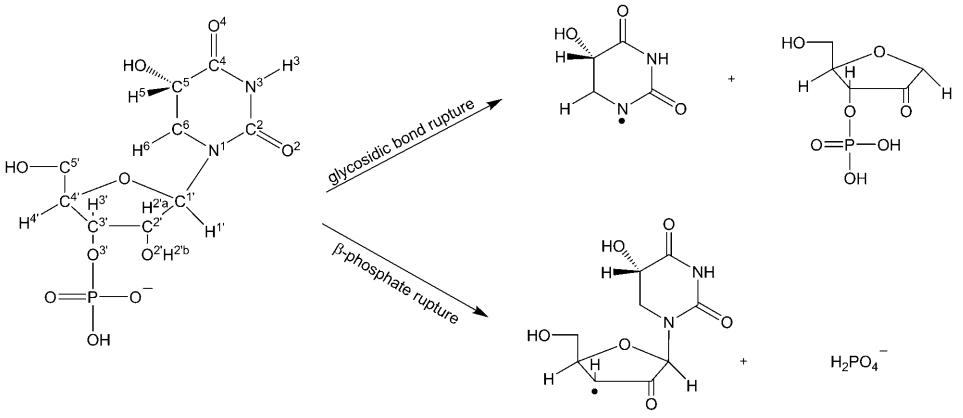

Scheme 2. Glycosidic and β-phosphate bond rupture of 3′-uridine monophosphate.

in RNA under radical stress. In addition, bulk solvation effects on the above processes are investigated.

Methodology

All geometries were optimized at the hybrid Hartee–Fock density functional theory B3LYP level[24,25] in conjunction with the 6-31+G(d,p) basis set. Frequency calculations were performed at the same level of theory to confirm the correct nature of the stationary points. For the N1–glycosidic bond rupture processes, the potential-energy surfaces (PESs) were scanned from the initial hydroxy-radical adducts by varying the N1−C1′ distance by using a step length of 0.1 Å and optimizing the remaining coordinates. The same procedure was used to determine the PES of β-phosphate bond dissociation of the radical adducts by scanning the C3′−O3′ distance. Bulk solvation effects were considered by using the integral equation formalism of the polarized continuum model (IEF-PCM)[26] by using the dielectric constant $\varepsilon = 78.4$ to model aqueous solution. To verify the trends, single-point calculations were also performed at the B3LYP/DZP++ level (Table 2).[21] The data obtained with the two basis sets turned out to be highly similar. Furthermore, gas-phase calculations were also performed by using the MPW1K functional of Truhlar and co-workers,[27] as this functional is reported to provide more-accurate kinetics. The data are, in this case, somewhat inconclusive (see Table 2), with differences in barrier heights within 1.5 kcal mol^{-1} for the first reaction steps involving hydrogen transfer. However, barrier heights differ as much as 5–9 kcal mol^{-1} for subsequent base release or strand-break steps. Similar trends are seen for the thermochemistry, in that the reaction energies are very similar for the hydrogen/proton transfer steps with the different functionals, whereas the bond-breakage reactions become approximately 5 kcal mol^{-1} more exothermic at the MPW1K level. All data discussed from here onwards will be at the B3LYP/6-31+G(d,p) level, bearing the above differences in mind. All calculations were performed by using the Gaussian 03 package.[28]

Atomic labeling used in the text and tables throughout refers to Scheme 2. The hydrogen atoms at C2′ of the sugar are labeled H2′$_a$ for that attached directly to C2′, and H2′$_b$ for the hydrogen attached to oxygen. The RNA strand was truncated by hydrogen atoms at the C5′OH and the C3′−O3′P(O)$_2^-$OH ends, and the phosphate was kept negatively charged to ensure an appropriate local environment. The use of a negatively charged phosphate group proved to be of importance to the results obtained, as will be discussed below.

Results and Discussion

Hydrogen transfer initiated by hydroxy-radical addition: Hydroxy-radical addition to 3′-UMP occurs primarily at the pyrimidine C5 position. Two cases are considered herein: hydroxy attack from the back and front at the C5 site of the base, as illustrated in Figure 1 (**B1**) and Figure 2 (**F1**), respectively. The energy difference between the two radical adducts is 4.6 kcal mol^{-1} in favor of the front adduct **F1**, owing to a more favorable interaction between the phosphate group and the ribose, and between the hydroxy group attached to C5 and the 2′-OH. The radical centers are, as expected, localized at C6 in both cases. The C5−C6, N1−C1′, and C3′−O3′ bond lengths are almost identical in **B1** and **F1**. In **B1**, the alcohol (O2′)H2′$_b$ hydrogen forms a weak hydrogen bond to O3′, the Mulliken charges of which are 0.40 and −0.78 e, respectively (presented in Table 1). In **F1**, the O2′−H2′$_b$ distance is elongated from the 0.98 Å found in **B1** to 1.02 Å, as H2′ (0.52 e) forms a strong short hydrogen bond

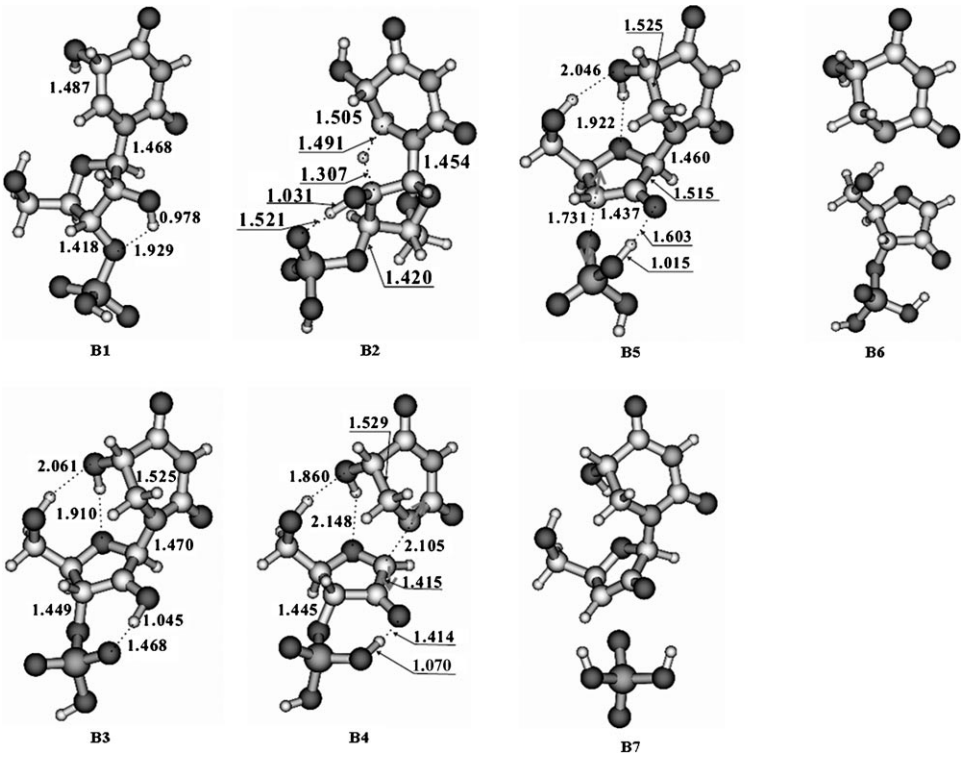

Figure 1. Selected geometrical parameters of the stationary structures along the hydrogen-atom abstraction and the subsequent base release and strand-breakage reactions (**B1**–**B 6**, **B1**– **B7**), obtained at the UB3LYP/6-31+G(d,p) level.

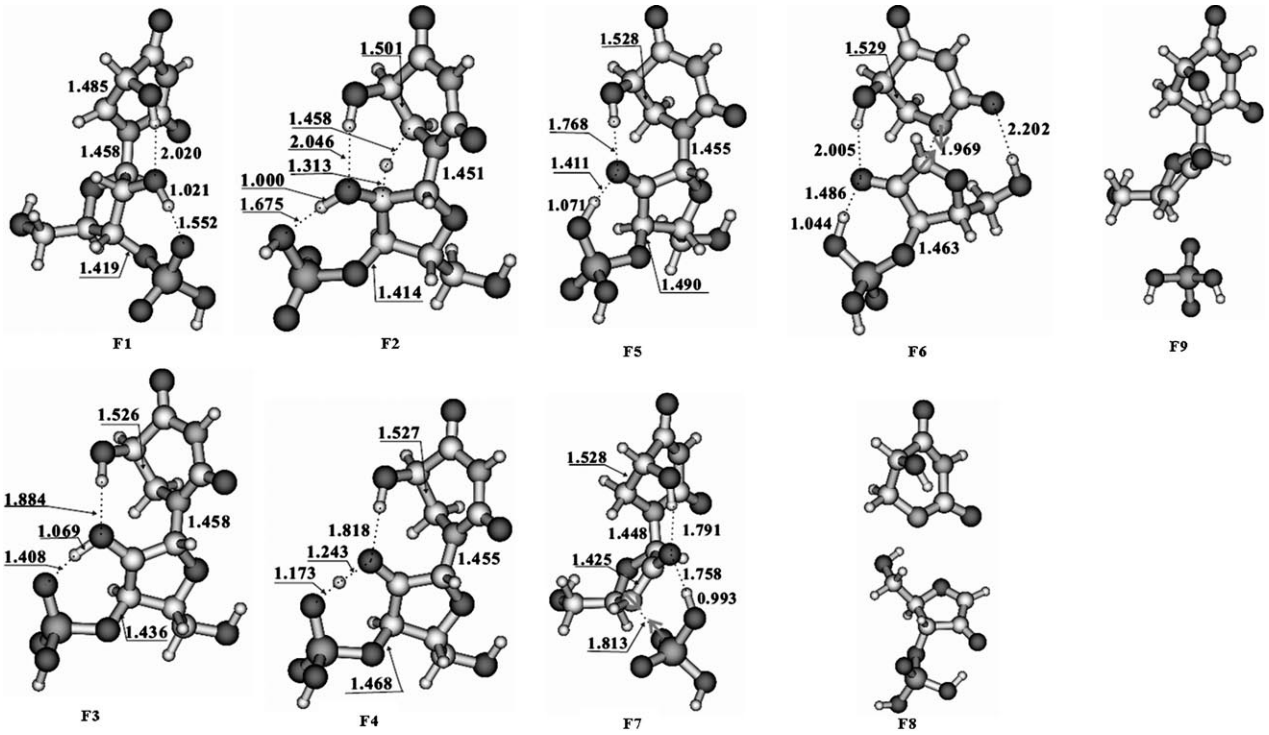

Figure 2. Selected geometrical parameters of the stationary structures along the hydrogen-atom abstraction and the subsequent base release and strand-breakage reactions (**F1**–**F8**, **F1**–**F9**), obtained at the UB3LYP/6-31+G(d,p) level.

Table 1. Mulliken charges (in e) of selected atoms in **B1** and **F1** obtained at the B3LYP/6-31+G(d,p) level.

	O5	O2′	O3′	H5′	H2′
B1	−0.46	−0.48	−0.78	0.35	0.40
F1	−0.51	−0.68	−0.95	0.44	0.52

to the negatively charged oxygen atom (−0.95 e) of the phosphate group. In addition, the charges of O5 and H5 are −0.46 and 0.35 e in **B1**, but −0.51 and 0.44 e in **F1**, respectively. These differences are attributed to the linear hydrogen bonding network O5H5···O2′H2′$_b$···O(P) occurring in **F1**, which contributes to the enhanced stability of the initial radical adduct. It is noted that the (O2′)H2′$_b$···O(P) distance in **F1** is 1.55 Å. This characterizes low-barrier hydrogen bonding (LBHB) and its significance for the reactions studied herein is addressed below.

During the H2′$_a$ transfer process, the C6···C2′ distance is shortened from 3.08 Å in **B1** to 2.56 Å in the H2′$_a$ transfer transition state (TS) **B2**. In the TS, the distances from H2′$_a$ to C6 and C2′ are 1.49 and 1.31 Å, respectively. The cyclic hydrogen-bonding network is also observed in **B3** (Figure 1). A rotation of the 3′ terminal PO_3H group in **B2** around the C3′−O3′ bond is noted; the rotation leads to the formation of a LBHB between 2′-OH and an oxygen atom of the phosphate group, with the distance 1.52 Å. In **B3**, the modified nucleobase becomes significantly puckered at the C5 and C6 atoms, enabling an additional hydrogen-bonding interaction to be formed between C5OH and the oxygen of the cyclic ribose ring.

A 3′-terminal PO_3H group rotation is also seen in **F2** (the hydrogen-transfer transition state), this time around the O3′−P bond. During the initial stage of the hydrogen-transfer process, the rotation results in 2′-OH forming a hydrogen bond with the 3′-terminal hydroxy oxygen rather than the negatively charged oxygen atom; after the TS, a reverse rotation occurs such that the hydrogen bond between 2′-OH and the negatively charged oxygen atom of the phosphate group is recovered. The rotation can be explained based on the charge redistribution that occurs during the H2′$_a$ transfer from C2′ to C6, enabling the linear hydrogen-bonding network to be retained. In **F2**, the distances of H2′$_a$ to C6 and C2′ are almost the same as in the case of **B2**. The change in the C6···C2′ distance during the reaction **F1**→**F2** is similar to that occurring in **B1**→**B2**.

The reaction energy profile is presented in Table 2 and Figure 3. The activation barrier in the gas phase for H2′$_a$ atom transfer to C6 is estimated to be 11.2 kcal mol^{-1} for **B1**→**B3**; approximately 8.8 kcal mol^{-1} lower than the **F1**→**F3** reaction. There is very little influence from bulk solvation. The results show that the local structural features governs the hydrogen-transfer reaction in a stereoselective way, that is, the hydrogen transfer is much preferred in the back radical adduct **B1** than in the front form. The difference in the barrier difference is attributed to the varied stability of the reactants **B1** and **F1** (**F1** being more stable by 4.6 kcal mol^{-1}) and the transition structures **B2** and **F2** (**B2**

Table 2. Computed reaction energies and activation barriers (in kcal mol^{-1}) for the intramolecular hydrogen-abstraction reactions and the subsequent strand-breakage reactions.

	B1→2→3		**B3→4→6**		**B3→5→7**	
Conditions	$\Delta E^{\neq}$	ΔE	$\Delta E^{\neq}$	ΔE	$\Delta E^{\neq}$	ΔE
a	14.7	−11.5	14.7	43.7	5.0	23.1
b	13.7	−11.4	15.4	44.4	5.5	24.9
c	14.4	−13.1	23.8	52.5	10.5	30.0
d	16.6	−6.9	21.4	29.2	5.5	−2.2
e	11.2	−11.3	12.4	32.5	4.0	20.3
f	12.2	−9.6	12.2	18.3	3.7	7.1
g	14.1	−6.6	18.4	12.6	3.9	−6.9

	F1→2→3		**F3→4→5**		**F5→6→8**		**F5→7→9**	
Conditions	$\Delta E^{\neq}$	ΔE	$\Delta E^{\neq}$	ΔE	$\Delta E^{\neq}$	ΔE	$\Delta E^{\neq}$	ΔE
a	22.6	−8.8	0.6	0.4	15.3	45.0	2.9	26.3
b	23.0	−8.8	0.5	0.5	16.0	46.0	3.7	28.0
c	24.5	−9.5	1.4	1.7	21.8	53.2	8.1	32.8
d	23.9	−9.2	2.6	3.4	21.4	28.4	2.8	−4.2
e	20.0	−9.4	−1.5	−0.3	15.0	35.6	3.2	24.5
f	20.2	−9.1	−1.5	−0.6	15.7	22.6	3.5	11.2
g	21.0	−9.7	0.5	2.6	20.4	12.4	2.3	−8.0

Conditions: a) Relative electronic energies at the B3LYP/6-31+G(d,p) level (not ZPE corrected). b) Relative electronic energies at the B3LYP/DZP++ level (not ZPE corrected). c) Relative electronic energies at the MPW1K/6-31+G(d,p) level (not ZPE corrected). d) In bulk solution (ε=78.4), B3LYP/DZP++ level. Not ZPE corrected. e) Relative electronic energies at the B3LYP/6-31+G(d,p) level (ZPE corrected) f) Changes in Gibbs free energies at 298 K in the gas phase. g) Relative electronic energies at the B3LYP/6-31+G(d,p) level in bulk solvent with ε=78.4, including ZPE correction.

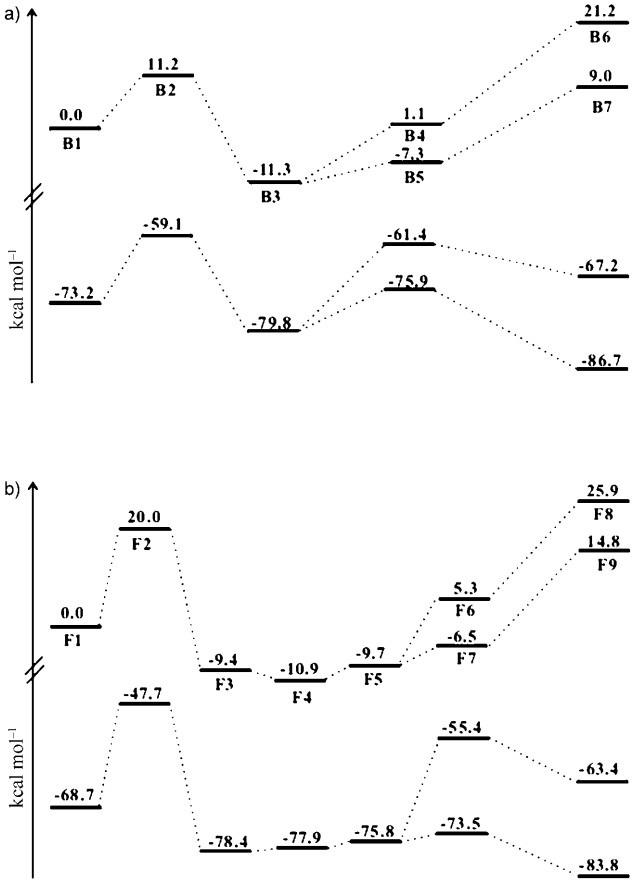

Figure 3. Energy profiles of the stationary structures along the hydrogen-atom abstraction and the subsequent base release and strand-breakage reactions, obtained at the (U)B3LYP/6-31+G(d,p) level. a) Back hydroxy-adduct reaction pathways; b) front hydroxy-adduct reaction pathways. In both (a) and (b), the top part is obtained in the gas phase and the lower part in solution with ε=78.4.

being favored over **F2** by 4.3 kcal mol^{-1}). The hydrogen-abstraction reactions **B1→2→3** and **F1→2→3** are exothermic by 11.3 and 9.4 kcal mol^{-1} in the gas phase and 6.6 and 9.7 kcal mol^{-1} in aqueous medium, respectively. The barriers and reaction energies are much lower than the values for H2′$_a$ transfer seen in both 3′dTMP and 5′dTMP,[16,17] respectively, which can be assigned to the effects of the hydrogen bonding interactions formed by 2′-OH.

In Table 3, we list the Mulliken unpaired spin densities on selected atoms in the sugar moieties along the reaction. As seen, the unpaired electron is highly localized to the C2′ (the "hydrogen abstracted") site; 0.87 e in **B3** and 0.81 e in **F5**.

Table 3. Mulliken atomic spin densities obtained at the B3LYP/6-31+G(d,p) level, of selected atoms along the reaction sequences.

	B3	**B4**	**B5**	**F5**	**F6**	**F7**
C1′	−0.137	0.264	−0.008	−0.118	0.129	−0.038
C2′	0.865	0.257	0.391	0.811	0.413	0.430
C3′	0.024	0.008	0.277	0.055	0.034	0.256
O of 2′-OH	0.168	0.249	0.234	0.195	0.238	0.227

C2′-radical-induced bond scission

N1–glycosidic bond rupture: The above H2′$_a$ transfer reactions result in a C2′-centered sugar radical, with the C1′−C2′ and C2′−C3′ distances being almost the same (1.49 Å) in the products **B3** and **F3**. The unpaired electron on C2′ can delocalize to the neighboring C1′−C2′ and C2′−C3′ bonds, leading to ruptures of the N1−C1′ and β-phosphate bonds, respectively. These are further enhanced by H2′$_b$-transfer reactions to nearby hydrogen-bond acceptors on the phosphate group, generating a carbonyl C2′=O2′ moiety, to be discussed in more detail below. The carboradical-induced ruptures of the N1−C1′ and β-phosphate bonds are explored at the B3LYP/6-31+G(d,p) level.

In the transition state **B4** of the N1−C1′ glycosidic bond rupture pathway from the radical intermediate **B3**, the N1···C1′ distance is 2.11 Å and its corresponding imaginary frequency is 122 cm^{-1}. In the reaction, (O2′-)H2′$_b$ proton transfer to the O(P) atom and formation of a C2′-centered carbonyl group occurs spontaneously at the very onset of the bond-rupture process. This is also reflected in the spin-density distribution (Table 3), according to which the unpaired electron is evenly distributed between C1′, C2′, and O2′ in the TS. This resonance stabilization of the product serves as a driving force for the base release reaction. The barrier of the **B3→4→6** reaction is 12.4 kcal mol^{-1} in the gas phase and 18.4 kcal mol^{-1} in bulk solution with ε=78.4 (see

Table 2). These values are considerably lower (by 8–12 kcal mol^{-1}) than the low-energy electron-induced barrier of N1···C1′ rupture in 3′dT and its mutant 3′-UMP(H).[21,29] The data show that the 2′-OH group of ribose significantly contributes to the decreased barrier of the N1−C1′ bond rupture found in the current work.

The structural characteristics of LBHB found in, for example, benzoylacetone has been discussed by Bruice and coworkers.[30] A similar LBHB formed by (O2′)H2′$_b$···O(P) is also found in **F3**. In this case, we observed a metastable C2′=O2′ carbonyl intermediate with the (O2′)H2′ transferred to the phosphate oxygen prior to C1′−N1 bond breakage. For the **F3**→**4**→**5** reaction, the zero point energy (ZPE)-corrected transition barrier of (O2′)H2′$_b$ transfer to an oxygen atom of the phosphate group is −1.5 kcal mol^{-1} in the gas phase and 0.5 kcal mol^{-1} in bulk solution. One of the reasons for the very low, and even negative, barrier is that the B3LYP method often underestimates barrier heights.[31] On the other hand, low barriers are characteristic of LBHB.[30] **F3** and **F5** have almost the same stability, with **F5** being slightly more stable (by 0.3 kcal mol^{-1}) in the gas phase. Bulk solvation increases the barrier, and the energetic difference between **F3** and **F5** is now 2.6 kcal mol^{-1} in favor of **F3**. The corresponding H2′$_b$ proton-transfer intermediate was never found for **B3** although several attempts to move (O2′)H2′$_b$ to an oxygen atom of the phosphate were made. In **F5**, the radical center is highly localized at C2′ (0.811 e), whereas in the TS **F6**, we note a delocalized spin-density distribution, albeit still with the main component in C2′, compared with the spin density at C1′ and O2′ (Table 3). The barrier of the **F5**→**6**→**8** ′N1-C1′ glycosidic bond breakage reaction is 15.0 kcal mol^{-1} in the gas phase and 20.4 kcal mol^{-1} in bulk solution (Table 2). These values are higher than those found in the **B3**→**4**→**6** reaction.

The PESs were scanned by varying the N1−C1′ distance stepwise from the radical adducts **B3** and **F3** and optimizing the remaining coordinates. We observed that (O2′)H2′$_b$ transfer to oxygen of phosphate occurs in **B3** with no barrier along the extension of N1−C1′ distance (see the Supporting Information). In fact, (O2′)H2′$_b$ is transferred to an oxygen atom of the phosphate group in the transition structures **B4** and **F6**. Thus, the products of the N1−C1′ decomposition reaction include the two fragments, base (B) and ribose + phosphate (RP), the latter of the form H_2PO_4. The N1−C1′ BDE and its bond-dissociation Gibbs free energies (ΔG) are calculated at the B3LYP/6-31+G(d,p) level. Heterolytic dissociation of the N1−C1′ bond leading to the formation of a neutral B radical and a negatively charged closed-shell RP moiety was found to be highly favored over homolysis, with BDE values of 32.5 (back) and 35.6 kcal mol^{-1} (front) in the gas phase (Table 4). Thermal effects at 298 K contribute towards the bond decomposition. Bulk solvation generates a further lowering of the heterolytic BDE and even larger effects are noted for the ΔG with −1.6 (back) and −0.6 kcal mol^{-1} (front). The N1−C1′ bond decomposition is hence an exothermic reaction at 298 K in aqueous solution. Both homolytic and heterolytic base release leads to the formation of a planar conjugated O5′-C1′-C2′-O2′ system in the sugar ring.

Table 4. Gas- and solution-phase BDEs and bond-dissociation free energies (ΔG; in kcal mol^{-1}) for base release.[a]

	back		front	
	Heterolytic[d]	Homolytic[e]	Heterolytic[d]	Homolytic[e]
BDE[b]	32.5	39.9	35.6	42.1
BDE[c]	12.6	24.6	12.4	24.3
ΔG[b]	18.3	25.6	22.6	28.5
ΔG[c]	−1.6	10.2	−0.6	10.7

[a] B3LYP/6-31+G(d,p) level; all values are ZPE-corrected. [b] In gas phase. [c] In solution; ε=78.4. [d] Hydroxy-modified uracil base is neutral. [e] Hydroxy-modified uracil base carries unit negative charge.

β-*phosphate bond rupture*: An alternative hydroxy-induced radical damage to 3′-UMP is that of β-phosphate bond breakage, leading to RNA strand break. For this process, the barrier 4.0 kcal mol^{-1} of the **B3**→**5**→**7** reaction must be overcome in the gas phase. Bulk solvation only reduces the barrier height to 3.9 kcal mol^{-1}. The C3′···O3′ distance is 1.73 Å in **B5** with an imaginary frequency of 256*i* cm^{-1}. The reaction energy is strongly endothermic in the gas phase and moderately exothermic under the effects of bulk solvation. Again, resonance stabilization serves as a driving force for the reaction, as seen already in the TS **B5** (Table 3).

C3′O3′ bond breakage in the **F5**→**7**→**9** reaction has a barrier of 3.2 kcal mol^{-1} in gas phase when including ZPE correction. Thermal corrections at 298 K leads to a slight increase of the barrier to 3.5 kcal mol^{-1}. Bulk solvation decreases the barrier by approximately 1 kcal mol^{-1}. The C3′···O3′ distance is 1.81 Å in **F7** and its corresponding imaginary frequency is 220*i* cm^{-1}. The reaction is also strongly endothermic in the gas phase, but exothermic in bulk solution. Also for this reaction, we note a delocalization of the unpaired spin density in the transition state **F7**, which is of similar magnitude to that seen for **B5** (Table 3). The heat of reaction is largely reduced upon the inclusion of thermal corrections. Thus, the barrier height of the β-phosphate bond rupture is considerably lower than what is found for the N1-glycosidic bond rupture.

A PES scan similar to that for glycosidic bond breakage is also made to investigate the process of β-phosphate bond rupture. Additionally, it was observed that the (O2′)H2′$_b$ transfers to an oxygen atom of the phosphate without any barrier. In contrast with the front system for the N1′−C1 bond breakage, in which (O2′)H2′$_b$ transfer occurs as a separate first step, in the case of the C3′−O3′ bond breakage, (O2′)H2′$_b$ is immediately transferred to the oxygen atom. Thus, the decomposition products include base + ribose (BR) and H_2PO_4 fragments. Three calculations of the bond rupture were carried out: 1) homolytic reaction leading to the formation of a neutral H_2PO_4 radical and a negatively charged closed shell BR moiety; 2) heterolytic reactions producing a positively charged H_2PO_4 fragment and a double negatively charged BR radical; 3) a negatively charged closed-shell H_2PO_4 molecule and a neutral BR radi-

cal. The obtained BDE and ΔG values are shown in Table 5. According to the present calculations, the second form of heterolytic β-phosphate bond dissociation leading to the formation of a neutral BR radical and a negatively charged closed shell H_2PO_4 is highly favored over homolysis and the first type of heterolysis. The preferred BDE values are 20.3 (back) and 24.5 kcal mol^{-1} (front) in the gas phase. Depending on the charged natures of the fragments, bulk solvation can reduce the BDE values up to −6.9 and −8.0 kcal mol^{-1}, respectively. When thermal corrections at 298 K and bulk solvation are included together, the ΔG values are further reduced to −20.2 and −21.3 kcal mol^{-1}, respectively.

Table 5. Gas- and solution-phase BDE and bond dissociation free energies (ΔG) (in kcal mol^{-1}) for strand breakage.[a]

	Leaving H_2PO_4 group					
		back			front	
	Homolytic[e]	Heterolytic 1	Heterolytic 2	Homolytic	Heterolytic 1	Heterolytic 2
BDE[b]	50.6	367.3	20.3	42.9	369.3	24.5
BDE[c]	40.7	191.5	−6.9	33.6	192.3	−8.0
ΔG[b]	37.6	353.8	7.1	30.4	356.6	11.2
ΔG[c]	27.7	178.0	−20.2	21.2	179.5	−21.3
	Leaving HPO_4 group					
		back			front	
	Homolytic[d]	Heterolytic 1	Heterolytic 2	Homolytic	Heterolytic 1	Heterolytic 2
BDE[b]	37.3	143.1	270.7	41.7	148.6	282.8
BDE[c]	16.7	130.2	34.8	15.5	133.2	35.4
ΔG[b]	24.5	130.1	257.4	28.8	135.4	269.3
ΔG[c]	3.9	117.3	21.5	2.6	120.0	21.9

[a] All values are corrected with ZPE_{gas}. [b] In the gas phase. [c] In solution with $\varepsilon = 78.4$. [d] Charge of HPO_4 fragment is **−1** in homolytic, **0** in heterolytic 1, **−2** in heterolytic 2, respectively. [e] Charge of H_2PO_4 fragment is **0** in homolytic, **1** in heterolytic 1, **−1** in heterolytic 2, respectively.

As mentioned above, (O2′)H2′ can form a LBHB to a negatively charged oxygen atom of the phosphate group and hence the role of the LBHB on reactions of β-phosphate bond rupture was explored in more detail. To this end, the HPO_4 group was thus assumed to be one of the decomposition products rather than H_2PO_4. The corresponding BDE and ΔG values from the corresponding homolytic and heterolytic processes were calculated and are listed in Table 5 for comparison. It is obvious that homolytic dissociation of β-phosphate bond is highly favored over heterolysis, as the former leads to the formation of a negatively charged HPO_4^- radical and a neutral closed-shell BR moiety. The BDE values of homolysis are 37.3 (back) and 41.3 kcal mol^{-1} (front) in the gas phase; much smaller than the ones from any of the two other heterolytic reactions. Bulk solvation reduce the BDE values by 20–26 kcal mol^{-1}. Thermal corrections at 298 K also favor the homolytic reaction but the effects are weaker than those of bulk solvation. When both are included, the ΔG values are largely reduced to 3.9 (back) and 2.6 kcal mol^{-1} (front). Compared with the results of heterolytic dissociation with the H_2PO_4 product, the data show that (O2′)H2′$_b$ is involved in the formation of LBHB and transferring to the negatively charged oxygen atom of phosphate group, is a strongly contributing factor to the hydroxy-radical-induced β-phosphate bond-rupture reaction and that β-phosphate bond rupture is the major pathway in gas and solution phases.

Conclusions

In the present work, hybrid DFT methods have been employed to investigate the potential RNA-scission processes induced by ·OH-radical addition to the C5 site of uracil in 3′-UMP. Geometries, charges, and reaction energies were obtained by using B3LYP together with the 6-31+G(d,p) and DZP++ basis sets in the gas phase, followed by energy calculations performed at the same levels in solution ($\varepsilon = 78.4$) by using the integral equation formalism-polarizable continuum model (IEF-PCM) to model bulk solvation. The barriers of subsequent (C2′-)H2′$_a$ abstraction by the C6 radical site range from 11.2 to 20.0 kcal mol^{-1} in the gas phase and 14.1 to 21.0 kcal mol^{-1} in aqueous solution, showing that the local structure governs the hydrogen-abstraction reaction in a stereoselective way. The H2′$_a$ transfer reactions are exothermic in both the gas phase and aqueous solution. These results are drastically different from the cases in 3′dTMP of DNA, and is attributed to the effects of the 2′-OH group in ribose. This can form LBHB to an oxygen of the C3′-bound phosphate enabling proton transfer with almost no barrier. This, in turn, contributes to the ruptures of the N1-glycosidic and β-phosphate bonds.

The hydrogen-abstraction reaction by the C6 nucleobase radical site leads to the formation of a C2′ radical on ribose, which induces the subsequent N1-glycosidic and β-phosphate ruptures. The barriers for cleavage of the N1−C1′ bonds range from 12.4 to 15.0 kcal mol^{-1} in the gas phase. The calculated BDE of the N1–glycosidic bonds furthermore support a homolytic bond-cleavage process and base release for all the radical adducts. Bulk solvation effects are unfavorable to the bond-rupture barrier, whereas these together with thermal corrections at 298 K markedly contribute to a significant lowering of the reaction energies. The N1-glycosidic bond dissociation (base release) is facilitated by the 2′-OH group and the simultaneous formation of π bonds between C1′−C2′ on the sugar and N1−C2 on the leaving base.

The barriers for cleavage of the β-phosphate bonds are 4.0 (back) and 3.2 (front) kcal mol^{-1}. These values are considerably lower than the those of the N1-glycosidic bond breakage and can be attributed to the formation of a LBHB from (O2′)H2′$_b$ to an oxygen atom of phosphate. The calculated bond-dissociation energies of the β-phosphate bonds

support a heterolytic bond-cleavage process with a negatively charged H_2PO_4 as leaving group for both the radical adducts. The solvent contributes slightly favorably to the bond rupture, and the corresponding reactions are exothermic in bulk aqueous solution. The thermal correction included favor the reactions further.

The present results show that the β-phosphate bond is more facile to be broken by hydroxy-radical addition to 3′-UMP. Bulk solvation and thermal corrections are major factors to the reduction of the reaction energies of the N1–glycosidic and β-phosphate bond ruptures, which is in agreement with the experimental results by von Sonntag and coworkers.[32] The presence of the 2′-OH group in the ribose moiety, with its tendency for proton transfer to the phosphate group, induces a lower stability in RNA compared with DNA towards oxidative stress, and provides insight to the evolutionary necessity of employing DNA for storage and transfer of genetic information.

Acknowledgements

The Swedish Science Research Council (VR) and the National Natural Science Foundation of China (Grant Nos. 20643007, 20703004), are gratefully acknowledged for financial support. We also acknowledge generous grants of computing time at the National supercomputing facilities in Linköping (NSC). Excellent Young Scholars Research Fund of Beijing Institute of Technology is also appreciated.

[1] C. Von Sonntag, H.-P. Schuchman, *Encyclopedia of Molecular Biology and Molecular Medicine, Vol. 3*, Wiley-VCH, Weinheim, **1996**.
[2] A.-O. Colson, M. D. Sevilla, *J. Phys. Chem.* **1995**, *99*, 13033.
[3] B. Halliwell, J. M. C. Gutteridge, *Free Radicals in Biology and Medicine*, Oxford University Press, Oxford, **1999**.
[4] G. Stein, J. Weiss, *Nature* **1948**, *161*, 650.
[5] B. Commoner, J. Townsend, G. E. Pake, *Nature* **1954**, *174*, 689.
[6] a) H. R. Drew, R. M. Wing, T. Takano, C. Broka, S. Tanaka, K. Itakura, R. E. Dickerson, *Proc. Natl. Acad. Sci. USA* **1981**, *78*, 2179; b) B. Balasubramanian, W. K. Pogozelski, T. D. Tullius, *Proc. Natl. Acad. Sci. USA* **1998**, *95*, 9738; c) M. J. Li, L. Liu, K. Wei, Y. Fu, Q. X. Guo, *J. Phys. Chem. B* **2006**, *110*, 13582.
[7] D. G. E. Lemaire, E. Bothe, D. Schulte-Frohlinde, *Int. J. Radiat. Biol.* **1984**, *45*, 351.
[8] M. C. R. Symons, *J. Chem. Soc. Faraday Trans. 1* **1987**, *83*, 1.
[9] D. Becker, M. D. Sevilla in *Advances in Radiation Biology, DNA and Chromatin Damage Caused by Radiation Vol. 17* (Eds.: J. T. Lett, W. K. Sinclair), Academic Press, New York, **1987**.
[10] E. Bothe, G. A. Qureshi, D. Schulte-Frohlinde, *Z. Naturforsch.* **1983**, *38c*, 1030.
[11] a) L. R. Karam, M. Dizdaroglu, M. G. Simic, *Radiat. Res.* **1988**, *116*, 210; b) D. J. Deeble, C. von Sonntag, *Int. J. Radiat. Biol.* **1984**, *46*, 247.
[12] a) K. Hildenbrand, G. Behrens, D. Schulte-Frohlinde, J. N. Herak, *J. Chem. Soc. Perkin Trans. 2* **1989**, 283; b) D. Schulte-Frohlinde, K. Hildenbrand in *Free Radicals in Synthesis and Biology* (Ed.: F. Minisci), Kluwer, Amsterdam, **1989**, 335; c) D. Schulte-Frohlinde, J. Opitz, H. Gomer, E. Bothe, *Int. J. Radiat. Biol.* **1985**, *48*, 397; d) J. R. Wagner, J. E. van Lier, L. J. Johnston, *Photochem. Photobiol.* **1990**, *52*, 333; e) C. M. Krishna, C. Decarroz, J. R. Wagner, J. Cadet, P. Riesz, *Photochem. Photobiol.* **1987**, *46*, 175.
[13] M. R. Barvian, R. M. Barkley, M. M. Greenberg, *J. Am. Chem. Soc.* **1995**, *117*, 4894.
[14] Q. Zhang, Y. Wang, *J. Am. Chem. Soc.* **2004**, *126*, 13287.
[15] I. Dabkowska, J. Rak, M. Gutowski, *Eur. Phys. J. D* **2005**, *35*, 429.
[16] R. B. Zhang, F. X. Gao, L. A. Eriksson, *J. Chem. Theory Comput.* **2007**, *3*, 803.
[17] R. B. Zhang, L. A. Eriksson, *J. Phys. Chem. B* **2006**, *110*, 23583.
[18] a) B. Boudaiffa, P. Cloutier, D. Hunting, M. A. Huels, L. Sanche, *Science* **2000**, *287*, 1658; b) M. A. Huels, B. Boudaiffa, P. Cloutier, D. Hunting, L. Sanche, *J. Am. Chem. Soc.* **2003**, *125*, 4467; c) Y. Zheng, P. Cloutier, D. J. Hunting, J. R. Wagner, L. Sanche, *J. Am. Chem. Soc.* **2004**, *126*, 1002; d) Y. Zheng, P. Cloutier, D. J. Hunting, L. Sanche, J. R. Wagner, *J. Am. Chem. Soc.* **2005**, *127*, 16592; e) F. Martin, P. D. Burrow, Z. Cai, P. Cloutier, D. Hunting, L. Sanche, *Phys. Rev. Lett.* **2004**, *93*, 068101.
[19] a) G. Hanel, S. Denifl, P. Scheier, M. Probst, B. Farizon, M. Farizon, E. Illenberger, T. D. Mark, *Phys. Rev. Lett.* **2003**, *90*, 188104; b) H. Abdoul-Carime, S. Gohlke, E. Illenberger, *Phys. Rev. Lett.* **2004**, *92*, 168103; c) S. Denifl, S. Ptasiǹska, M. Cingel, S. Matejcik, P. Scheier, T. D. Mark, *Chem. Phys. Lett.* **2003**, *377*, 74; d) S. Ptasińska, S. Denifl, P. Scheier, E. Illenberger, T. D. Mark, *Angew. Chem.* **2005**, *117*, 7101; *Angew. Chem. Int. Ed.* **2005**, *44*, 6941; e) I. Bald, J. Kopyra, E. Illenberger, *Angew. Chem.* **2006**, *118*, 4969; *Angew. Chem. Int. Ed.* **2006**, *45*, 4851; f) C. König, J. Kopyra, I. Bald, E. Illenberger, *Phys. Rev. Lett.* **2006**, *97*, 018105; g) S. Denifl, S. Ptasińska, M. Probst, J. Hrusak, P. Scheier, T. D. Mark, *J. Phys. Chem. A* **2004**, *108*, 6562; h) S. Ptasiǹska, S. Denifl, B. Mroz, M. Probst, V. Grill, E. Illenberger, P. Scheier, T. D. Mark, *J. Chem. Phys.* **2005**, *123*, 124302.
[20] a) R. Barrios, P. Skurski, J. Simons, *J. Phys. Chem. B* **2002**, *106*, 7991; b) J. Berdys, I. Anusiewicz, P. Skurski, J. Simons, *J. Phys. Chem. A* **2004**, *108*, 2999; c) J. Berdys, P. Skurski, J. Simons, *J. Phys. Chem. B* **2004**, *108*, 5800; d) I. Anusiewicz, J. Berdys, M. Sobczyk, P. Skurski, J. Simons, *J. Phys. Chem. A* **2004**, *108*, 11381; e) J. Berdys, I. Anusiewicz, P. Skurski, J. Simons, *J. Am. Chem. Soc.* **2004**, *126*, 6441; f) J. Simons, *Acc. Chem. Res.* **2006**, *39*, 772.
[21] a) J. Gu, Y. Xie, H. F. Schaefer, *J. Am. Chem. Soc.* **2005**, *127*, 1053; b) X. Bao, J. Wang, J. Gu, J. Leszczynski, *Proc. Natl. Acad. Sci. USA* **2006**, *103*, 5658; c) J. Gu, J. Wang, J. Leszczynski, *J. Am. Chem. Soc.* **2006**, *128*, 9322; d) J. Gu, Y. Xie, H. F. Schaefer, *J. Am. Chem. Soc.* **2006**, *128*, 1250; e) J. Gu, Y. Xie, H. F. Schaefer, *J. Phys. Chem. B* **2006**, *110*, 19696.
[22] a) X. Li, M. D. Sevilla, L. Sanche, *J. Phys. Chem. B* **2004**, *108*, 19013; b) Z. Cai, M. D. Sevilla, *Top. Curr. Chem.* **2004**, *237*, 103; c) X. Li, M. D. Sevilla, *Adv. Quantum Chem.* **2007**, *52*, 59; d) A. Kumar, M. D. Sevilla, *J. Phys. Chem. B* **2007**, *111*, 5464.
[23] E. Westhof, *Science* **1999**, *286*, 61.
[24] A. D. Becke, *J. Chem. Phys.* **1993**, *98*, 5648.
[25] C. Lee, W. Yang, R. G. Parr, *Phys. Rev. B* **1988**, *37*, 785.
[26] J. Tomasi, M. Persico, *Chem. Rev.* **1994**, *94*, 2027.
[27] B. J. Lynch, P. L. Fast, M. Harris, D. G. Truhlar, *J. Phys. Chem. A* **2000**, *104*, 4811.
[28] Gaussian 03, Revision B.04, M. J. Frisch, G. W. Trucks, H. B. Schlegel, G. E. Scuseria, M. A. Robb, J. R. Cheeseman, J. A. Montgomery, Jr., T. Vreven, K. N. Kudin, J. C. Burant, J. M. Millam, S. S. Iyengar, J. Tomasi, V. Barone, B. Mennucci, M. Cossi, G. Scalmani, N. Rega, G. A. Petersson, H. Nakatsuji, M. Hada, M. Ehara, K. Toyota, R. Fukuda, J. Hasegawa, M. Ishida, T. Nakajima, Y. Honda, O. Kitao, H. Nakai, M. Klene, X. Li, J. E. Knox, H. P. Hratchian, J. B. Cross, C. Adamo, J. Jaramillo, R. Gomperts, R. E. Stratmann, O. Yazyev, A. J. Austin, R. Cammi, C. Pomelli, J. W. Ochterski, P. Y. Ayala, K. Morokuma, G. A. Voth, P. Salvador, J. J. Dannenberg, V. G. Zakrzewski, S. Dapprich, A. D. Daniels, M. C. Strain, O. Farkas, D. K. Malick, A. D. Rabuck, K. Raghavachari, J. B. Foresman, J. V. Ortiz, Q. Cui, A. G. Baboul, S. Clifford, J. Cioslowski, B. B. Stefanov, G. Liu, A. Liashenko, P. Piskorz, I. Komaromi, R. L. Martin, D. J. Fox, T. Keith, Al-Laham, M. A.; C. Y. Peng, A. Nanayakkara, M. Challacombe, P. M. W. Gill, B. Johnson, W. Chen, M. W. Wong, C. Gonzalez, J. A. Pople, Gaussian, Inc., Pittsburgh, PA, **2003**.
[29] R. B. Zhang, K. Zhang, L. A. Eriksson, *Chem. Eur. J.* **2008**, *14*, 2850.

[30] B. Schiøtt, B. B. Iversen, G. H. Madsen, F. K. Larsen, T. C. Bruice, *Proc. Natl. Acad. Sci. USA* **1998**, *95*, 12799.
[31] Y. Zhao, N. González-García, D. G. Truhlar, *J. Phys. Chem. A* **2005**, *109*, 2012.
[32] D. J. Deeble, D. Schulz, C. von Sonntag, *Int. J. Radiat. Biol.* **1986**, *49*, 915.

Received: August 11, 2008
Revised: October 20, 2008
Published online: January 20, 2009

